Table 4 Summary of experimental results at 298.15 K (cal_{th} = 4.184 J)

	$(\Delta E_c^\circ/M)/cal_{th}\ g^{-1}$			
	exo-THDC	RJ-4	RJ-4-I	JP-9
	−10685.70	−10776.90	−10764.86	−10672.39
	81.04	74.78	64.27	68.70
	79.84	76.04	66.10	69.55
	83.59	76.14	63.12	66.80
	81.37	77.91	62.46	70.40
	−10680.53	−10772.28	−10762.78	−10668.28
Mean	−10682.01	−10775.68	−10763.93	−10669.35
Standard deviation of the mean	0.90	0.80	0.57	0.78

Table 5 Derived molar values for the liquid state at 298.15 K (cal_{th} = 4.184 J)

Fuel	ΔE_c°, $kcal_{th}\ mol^{-1}$	ΔH_c°, $kcal_{th}\ mol^{-1}$	ΔH_f°, $kcal_{th}\ mol^{-1}$
exo-THDC	−1455.31 ± 0.33	−1457.68 ± 0.33	−29.35 ± 0.35
RJ-4	−1770.37 ± 0.37	−1773.33 ± 0.37	−38.43 ± 0.40
RJ-4-I	−1768.44 ± 0.36	−1771.40 ± 0.36	−40.36 ± 0.39
JP-9	−1523.55 ± 0.34	−1525.95 ± 0.34	----------

values of ΔH_f° refer to Eqs. (2) and (4). The uncertainties given in Table 5 are the "uncertainty intervals."[13] The enthalpies of formation of CO_2(g) and H_2O(l) were taken to be −94.051 and −68.315 $kcal_{th}\ mol^{-1}$, respectively.[14] Uncertainties assigned to the respective values were 0.011 $kcal_{th}\ mol^{-1}$ for CO_2[15] and 0.010 $kcal_{th}\ mol^{-1}$ for H_2O(l).[16]

The values of enthalpy of combustion given in Tables 3-5 are the "gross" heats of combustion for which the reaction products are gaseous carbon dioxide and liquid water. For combustion yielding gaseous carbon dioxide and gaseous water, the values of the "net" heat of combustion are: *exo*-THDC, −(10081.5 ± 2.3) cal g^{-1}; RJ-4, −(10153.1 ± 2.3) cal g^{-1}; RJ-4-I, −(10141.7 ± 2.2) cal g^{-1}; and JP-9, −(10089.5 ± 2.4) cal g^{-1}.

Acknowledgment

The authors gratefully acknowledge the assistance of S. Lee-Bechtold who measured heat capacities of the fuel samples. This work was conducted under an Interagency Agreement, AFOSR-ISSA-78-0009, between the Air Force Office of Scientific Research (AFSC) and the Department of Energy.

References

[1] Good, W.D., "The Enthalpies of Combustion and Formation of Some Alkyl Cyclopropanes," *Journal of Chemical Thermodynamics*, Vol. 3, July 1971, pp. 539-546.

[2] Good, W.D., Moore, R.T., Osborn, A.G., and Douslin, D.R., "The Enthalpies of Formation of Ethylcyclobutane, Methylenecyclobutane, and 1,1-Dimethylcyclopropane," *Journal of Chemical Thermodynamics*, Vol. 6, March 1974, pp. 303-310.

[3] Good, W.D., and Lee, S.H., "The Enthalpies of Formation of Selected Napthalenes, Diphenylmethanes, and Bicyclic Hydrocarbons," *Journal of Chemical Thermodynamics*, Vol. 8, July 1976, pp. 643-650.

[4] Good, W.D., "The Enthalpies of Formation of Some Bridged-Ring Polynuclear Aromatic Hydrocarbons," *Journal of Chemical Thermodynamics*, Vol. 10, June 1978, pp. 553-558.

[5] Hubbard, W.N., Scott, D.W., and Waddington, G., "Standard States and Corrections for Combustions in a Bomb at Constant Volume," *Experimental Thermochemistry*, Interscience, New York, 1956, Chap. 5, pp. 75-128.

[6] Goof, W.D. and Smith, N.K., "The Enthalpies of Combustion of Toluene, Benzene, Cyclohexane, Cyclohene, Methylcyclopentane, 1-Methylcyclopentene, and n-Hexane," *Journal of Chemical and Engineering Data*, Vol. 14, Jan. 1969, pp. 102-106.

[7] Good, W.D., "The Enthalpies of Combustion and Formation of 11 Isomeric Nonanes," *Journal of Chemical and Engineering Data*, Vol. 14, April 1969, pp. 231-235.

[8] Good, W.D., Scott, D.W., and Waddington, G., "Combustion Calorimetry of Organic Flourine Compounds by a Rotating-Bomb Method," *Journal of Physical Chemistry*, Vol. 60, Aug. 1956, pp. 1080-1089.

[9] Good, W.D. et al., "Thermochemistry and Vapor Pressure of Aliphatic Fluorocarbons. A Comparison of the C-F and C-H Thermochemical Bond Energies," *Journal of Physical Chemistry*, Vol. 63, July 1959, pp. 1133-1138.

[10] Guthrie, G.B., Jr., et al., "Thermodynamic Properties of Furan," *Journal of the American Chemical Society*, Vol. 74, Sept. 1952, pp. 4662-4669.

[11] Cameron, A.E., and Wichers, E., "Report of the International Commission on Atomic Weights (1961)," *Journal of the American Chemical Society*, Vol. 84, Dec. 1962, pp. 4175-4197.

[12] Cohen, E.R., and DuMond, J.W.M., "Our Knowledge of the Fundamental Constants of Physics and Chemistry in 1965," *Reviews of Modern Physics*, Vol. 37, Oct. 1965, pp. 537-594.

[13] Rossini, F.D., "Assignment of Uncertainties to Thermochemical Data," *Experimental Thermochemistry*, Interscience, New York, 1956, Chap. 14, pp. 297-320.

[14] Wagman, D.D., Evans, W.H., Halow, I., Parker, V.B., Bailey, S.M., and Shumm, R.H., "Selected Values of Chemical Thermodynamic Properties," National Bureau of Standards (U.S.) Technical Note 270-3, U.S. Government Printing Office, Washington, D.C., Jan. 1968.

[15] Rossini, F.D., and Jessup, R.S., "Heat and Free Energy of Formation of Carbon Dioxide, and of the Transition Between Graphite and Diamond," *Journal of Research of the National Bureau of Standards*, Vol. 21, Oct. 1938, pp. 491-513.

[16] Rossini, F.D., "The Heat of Formation of Water," *Journal of Research of the National Bureau of Standards*, Vol. 6, Jan. 1931, pp. 1-35.

Artificially Thickening a Smooth-Wall Turbulent Boundary Layer

Phillip M. Ligrani* and Robert J. Moffat†
Stanford University, Stanford, Calif.

Introduction

THE ability to thicken a turbulent boundary layer artificially gives the investigator a way to obtain thick layers in short wind tunnel distances, and thus expand the experimental operating domain of a wind tunnel without the high cost of increasing the length of the test surface. One must prove, however, that the thickened boundary layer has the

Received Sept. 11, 1978; revision received Feb. 26, 1979.

Index categories: Boundary Layers and Convective Heat Transfer—Turbulent; Hydrodynamics; Atmospheric and Space Sciences.

*Graduate Research Assistant, Dept. of Mechanical Engineering.

†Professor and Chairman, Thermosciences Division, Dept. of Mechanical Engineering.

same properties as would a naturally developed boundary layer of the same thickness. The turbulent transport properties then have normal characteristics which allow the flowfield to be used for research purposes. Artificially thickened boundary layers have been made before, but usually to simulate atmospheric boundary layers[1] or to model flat-plate boundary-layer information only up to first-order information.[2] An exception is the technique of Klebanoff and Diehl,[3] which produces a flowfield with normal characteristics to the level of one-dimensional $\overline{u'^2}$ spectra, but produces only small increases in the thickness. The present technique was then developed with the objective of producing flowfields whose mean and turbulence properties would be closely similar to those of naturally developing flows and, at the same time, provide substantial thickness increases.

Design of Artificial Thickening Device

The apparatus used to produce the augmented boundary layer is shown in Fig. 1, and consists of two basic components: an array of spires and a barrier. The flow from the wind tunnel nozzle first passes by the spires and then the barrier, both of which extend across the width of the wind tunnel at the upstream end of the test surface. The flow produced by the present device is examined at only one freestream velocity. However, a slightly modified version of the present smooth-wall design is demonstrated to be useful for rough-wall boundary layers for freestream velocities ranging from 9 to 28 m/s.[4] The spire configuration, shown in Fig. 1, was developed from a design described by Peterka and Cermak[1] which had been used to simulate atmospheric boundary layers.

The flow properties in the thickened boundary layer depend on the geometric characteristics of the array of spires and barrier. The total thickness of the boundary layer just downstream of the thickening apparatus, δ, is directly proportional to the height of the spires, β. The momentum thickness at the same location can be expressed as $\delta_2 = (C_D/2)(A_f/\omega)$, where C_D is the drag coefficient of the spires based on spire frontal area A_f and ω is defined on Fig.

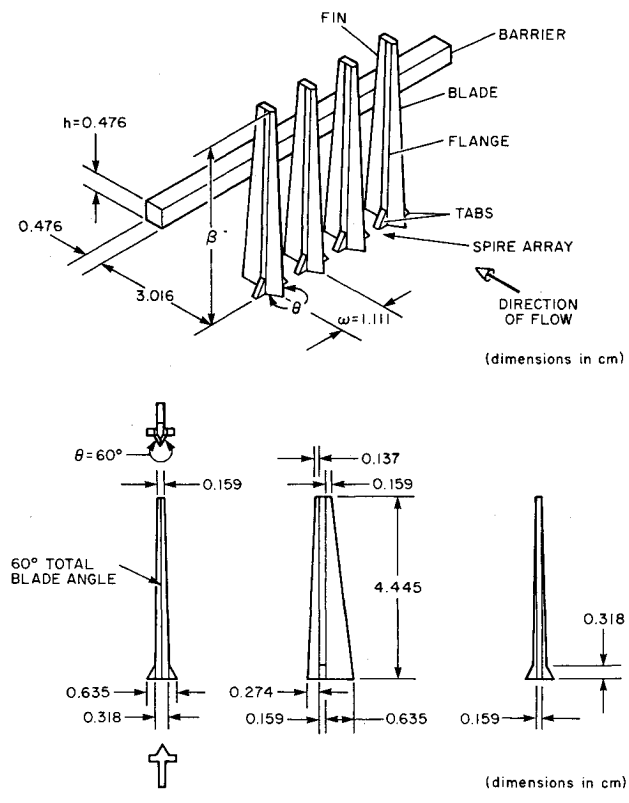

Fig. 1 Artificial thickening apparatus.

1. Altering C_D by streamlining the spires using sharp-edged upstream and downstream blades alters the velocity distribution in the wake of the augmented boundary layer. A control volume analysis indicates that the total angle of the upstream blade θ can also be varied for fine adjustment of the velocity profiles. In addition, the upstream blades have important effects on turbulent fluctuation intensities. The upstream blades divert fluid away from the centerlines of the spires, to mix with fluid diverted from adjacent spires. The amount of this mixing, dependent on θ, then affects turbulence levels just downstream of the spires and, therefore, levels at measuring stations further downstream.

The barrier shown in Fig. 1 greatly increases the momentum deficit over that produced by the spires alone. By changining the barrier height h, the relation between the mean velocity and skin friction can also be changed to obtain agreement with the law of the wall.

Thick Boundary-Layer Characteristics

Using the apparatus described, the integral quantities, mean velocity profiles, and turbulence structure in the artifically thickened boundary layer resemble natural data downstream of the thickening apparatus.

The following data are intended to show that the augmented boundary layer is of "normal character."

Integral Properties

The data for displacement thickness and momentum thickness agree with the correlations of Schultz-Grunow[5] for $x_1 > 0.9$ m, where x_1 is the longitudinal distance downstream of the artificial thickening apparatus. The effective hydrodynamic starting length upstream of the thickening apparatus, L, was determined to be 2.60 m, based on the displacement thickness correlation of Schultz-Grunow.

Skin Friction

The local values of skin friction coefficient in the artificially thickened boundary layer were determined from near-wall measurements of the Reynolds shear stress made using a rotatable, slanted, hot-wire anemometer ($C_f/2 \simeq -\overline{u'v'}/u_\infty^2$ at $y = 0.330$ cm). Results of these measurements indicate that the measured skin friction agrees with the Schultz-Grunow correlation, calculated using the same L discussed previously. The data also agree with $C_f/2 = 0.0128 (Re_{\delta_2})^{-0.25}$, where Re_{δ_2} is the momentum thickness Reynolds number, which ranges from 4100-5700 in the present study. For $x_1 > 0.9$ m, the measured skin friction coefficients are closely similar to values determined from the velocity profiles using a "Clauser plot."[6] Agreement with the moment integral equation for average skin friction is maintained within 10% at the same locations.

Mean Velocity Profiles—Inner Coordinates

Velocity profiles in wall coordinates are shown in Fig. 2. These profiles were nondimensionalized using values of the friction velocity u_τ determined from measured skin friction, and for $x_1 > 0.9$ m show excellent agreement with the law of the wall

$$u^+ = (1/\kappa) \ln y^+ + C \tag{1}$$

where $\kappa = 0.41$ and $C = 5.10$. The value of y^+ at which the data begin to deviate from the law of the wall (near the wake) is approximately 500, which is consistent with Clauser's[8] observation for a momentum thickness Reynolds number of 5000. Figure 2 also indicates that in the transition region of the artificially thickened boundary layer, the velocity measurements fall within the scatter of Laufer's[7] data for pipe flow.

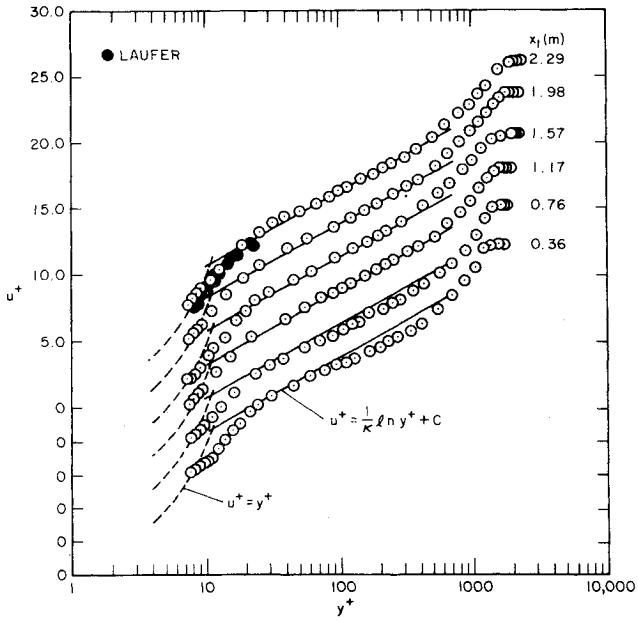

Fig. 2 Downstream development of velocity profiles in boundary-layer coordinates.

Clauser Equilibrium and Mean Velocity Profiles—Outer Coordinates

The artificially thickened boundary layer evidently reaches a Clauser[8]-type equilibrium for $x_1 > 0.9$ m, since the Clauser shape factor G becomes constant at approximately 6.8, a value consistent with natural zero pressure gradient boundary-layer behavior. Consequently, the measured velocity profiles in defect coordinates are similar at different downstream locations. Agreement is also maintained with Coles'[9] law of the wake

$$\frac{u_\infty - u}{u_\tau} = -\frac{1}{\kappa} \ell n\left(\frac{y}{\delta}\right) + \frac{\pi}{\kappa}\left[2 - \omega\left(\frac{y}{\delta}\right)\right] \qquad (2)$$

where $\pi = 0.55$ for zero pressure gradient flows, $\omega(n)$ is Coles' wake function, $\kappa = 0.41$, δ is the boundary-layer thickness, and u_∞ is the freestream velocity. The fricition velocities used to nondimensionalize experimental profiles for comparison with Eq. (2) were determined from measured values of local skin friction. A spanwise mean velocity profile survey at $x_1 = 1.22$ m ($z = -5.08$ cm, $z = 0$ cm (centerline), and $z = 10.16$ cm) showed a variation of momentum thickness of less than 3% about the mean.

Turbulence

The profiles of longitudinal turbulent intensity, turbulent shear stress $-\overline{u'v'}$, and turbulent kinetic energy $\overline{q^2}$, are closely similar to those of naturally developing boundary layers at $x_1 = 1.98$ m and $x_1 = 2.29$ m. Profiles of $\overline{q^2}/u_\tau^2$ and $-\overline{u'v'}/u_\tau^2$ vs y/δ at four downstream locations are shown in Fig. 3, along with Klebanoff's[10] measurement for comparison. The slight deficits which exist for $0.14 < y/\delta < 0.50$ at $x_1 = 1.17$ m and at $x_1 = 1.57$ m disappear farther downstream, where longitudinal similarity of the profiles develops. Turbulence data in the artifically thickened boundary layer also show agreement (for $0.10 < y/\delta < 0.90$) with the cross-correlation coefficient for the turbulent shear stress and the Reynolds shear stress-turbulent kinetic energy ratio within $\pm 10\%$, where the correlations are:

$$-\overline{u'v'}/\sqrt{\overline{u'^2}\,\overline{v'^2}} = 0.46 \text{ and } -\overline{u'v'}/\overline{q^2} = 0.145 \qquad (3)$$

Spectra

No spectral measurements were made in the smooth-wall, artificially thickened boundary layer of the present study.

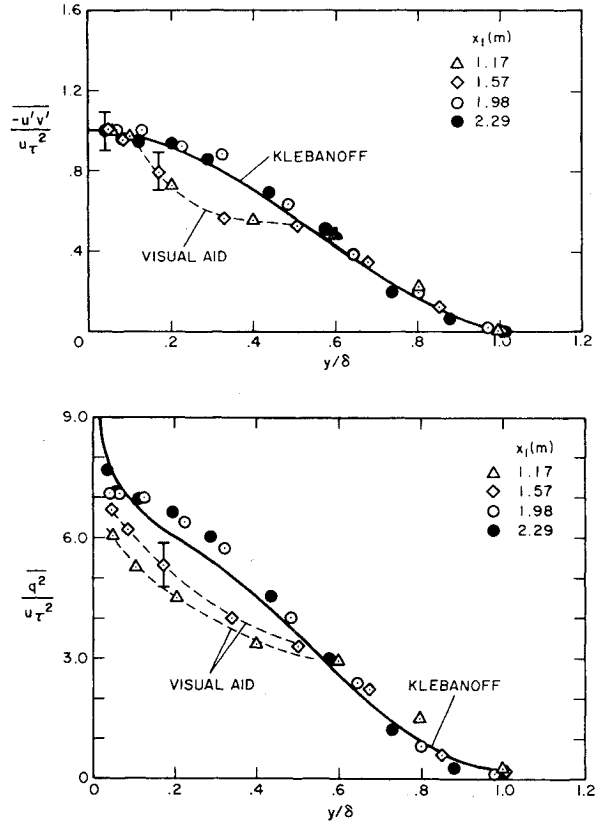

Fig. 3 Downstream development of turbulence properties.

Spectra of the longitudinal velocity fluctuations taken in a thickened boundary layer produced over a rough surface using a slightly modified version of the Fig. 1 design are presented by Ligrani.[4] Results indicate that the normalized spectra, scaled on boundary-layer thickness, for $y/\delta = 0.078$, 0.150, and 0.600 show excellent agreement with measurements from naturally developing flows.

Wind Tunnel and Measurement Techniques

The artificially thickened boundary layer was developed in the HMT-1 heat-transfer tunnel at Stanford, which has been described by Moffat.[11] The smooth test surface of the wind tunnel is 2.44 m long and 0.508 m wide. The mean velocities u were measured using a boundary-layer pitot probe in conjunction with a micromanometer. The Reynolds stress tensor components were measured using horizontal and rotatable slanted hot-wire probes. The pitot probe and the two hot-wire probes were mounted on individual traversing mechanisms, each with a micrometer for adjustment of probe position relative to the wall. All profile measurements were made on the centerline of the tunnel, $z = 0$, except when spanwise uniformity checks of the mean velocity were made.

Conclusions

Measurements in an artificially thickened flowfield in air at $u_\infty = 10.1$ m/s with $T_\infty \sim 23°C$ indicate that it is possible to create a hydrodynamic field similar to thick, smooth-wall, turbulent boundary layers. The augmented layer develops naturally in a zero pressure gradient to the level of the cross-correlation coefficient based upon the turbulent shear stress and the Reynolds shear stress-turbulent kinetic energy ratio. The effective length of the wind-tunnel test section is increased by 2.60 m, and the displacement thickness is increased by a factor of 1.74 over the hydrodynamic flowfield which would develop naturally on the downstream end of the same test surface.

Tabular data listings and additional details of the artificial thickening design, experimental apparatus, measurement techniques, and qualification tests are given by Ligrani.[4]

Acknowledgments

The authors gratefully acknowledge the many helpful comments and suggestions of J. P. Johnston with regard to this research effort. This work was supported by the Office of Naval Research, Contracts N00014-67-A-0112-0072 and N00014-76-C-0532. The authors wish to thank J. Patton for his support.

References

[1] Peterka, J.A. and Cermak, J.E., "Simulation of Atmospheric Flows in Short Wind Tunnel Test Sections," CER73-74JAP-JEC32, Fluid Mechanics Program, Colorado State University, June 1974.

[2] Otten, III, L.J., and Van Kuren, J.T., "Artificial Thickening of High Subsonic Mach Number Boundary Layers," *AIAA Journal*, Vol. 14, Nov. 1976, pp. 1528-1533.

[3] Klebanoff, P.S. and Diehl, Z.W., "Some Features of Artificially Thickened Fully Developed Turbulent Boundary Layers with Zero Pressure Gradient," NACA Rept. 1110, 1952.

[4] Ligrani, P.M., Moffat, R.J., and Kays, W.M., "The Thermal and Hydrodynamic Behavior of Thick, Rough-Wall, Turbulent Boundary Layers," Rept. No. HMT-29, Thermosciences Div., Dept. of Mechanical Engineering, Stanford University, 1979.

[5] Schultz-Grunow, F., "New Frictional Resistance Law for Smooth Plates," NACA TM 986, Sept. 1941.

[6] Clauser, F.H., "Turbulent Boundary Layers in Adverse Pressure Gradients," *Journal of the Aeronautical Sciences*, Vol. 21, 1954, p. 91.

[7] Laufer, J., "The Structure of Turbulence in Fully Developed Pipe Flow," NACA Rept. 1174, 1954.

[8] Clauser, F.H., "The Turbulent Boudnary Layer," *Advances in Applied Mechanics*, Vol. IV, Academic Press, New York, 1956, pp. 1-51.

[9] Coles, D., "The Law of the Wake in the Turbulent Boundary Layer," *Journal of Fluid Mechanics*, Vol. 1, 1956, pp. 191-226.

[10] Klebanoff, P.S., "Characteristics of Turbulence in a Boundary Layer with Zero Pressure Gradient," NACA TN 3178, 1954.

[11] Moffat, R.J. and Kays, W.M., "The Turbulent Boundary Layer on a Porous Plate: Experimental Heat Transfer with Uniform Blowing and Suction," Rept. No. HMT-1, Thermosciences Div., Dept. of Mechanical Engineering, Stanford University, 1967.

Real-Time Optical Measurement of Time-Dependent Shock Position

M. Sajben* and R.C. Crites†

McDonnell Douglas Corporation, St. Louis, Mo.

Introduction

In the study of unsteady flows that contain oscillating shocks, it is desirable to obtain a real-time analog signal representing the streamwise position of the shock. Such a signal permits recording of shock position simultaneously with other time-dependent data (pressures, velocities, etc.). Simultaneous recording insures a precisely indexed time base for all signals and allows reliable computation of joint statistical properties, such as cross-correlations or conditionally averaged flow properties, using shock position as the trigger signal. In addition, the availability of on-line display of time-mean shock position provides the experimental convenience of taking data at preset shock positions.

Description of Apparatus

In a recent experimental study,[1] the need just outlined was met by incorporating a line-scan television camera in the conventional shadowgraph system of the flow facility, and

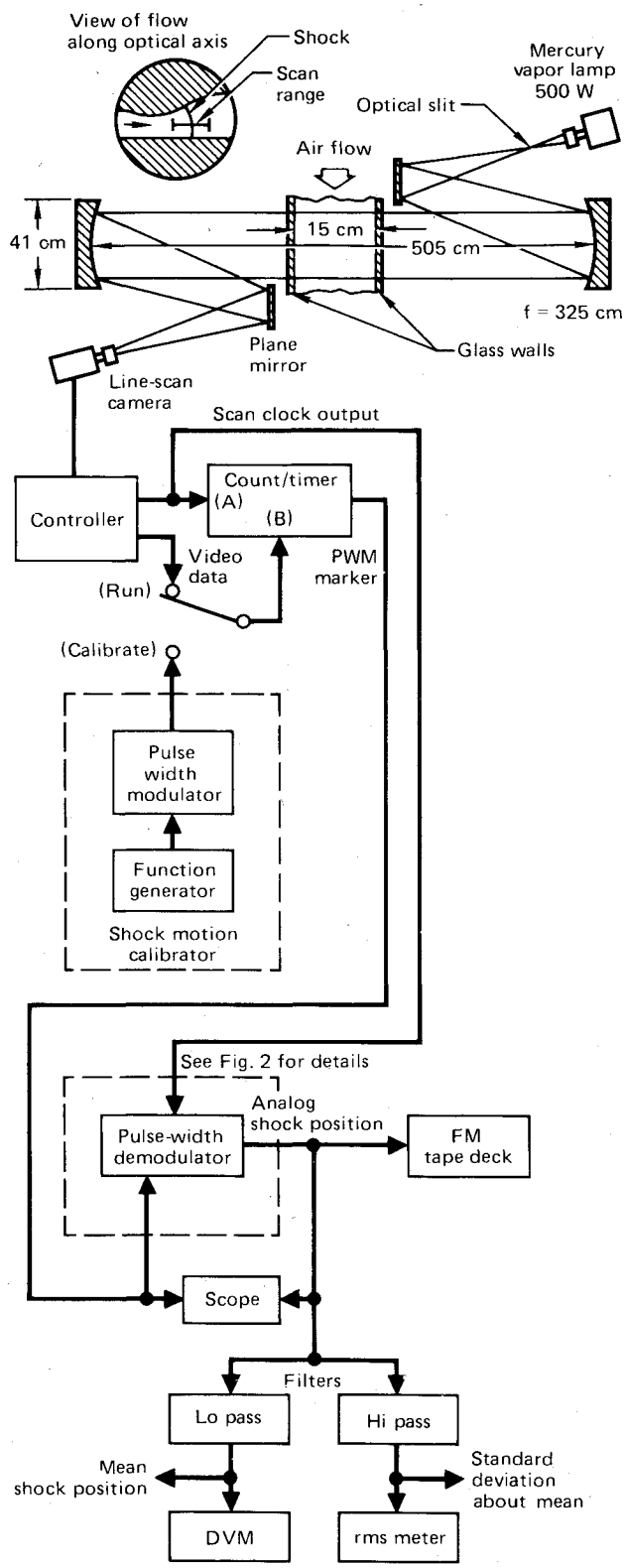

Fig. 1 Layout of shadowgraph system and schematic of electronics for line-scan data processing.

Received Jan. 8, 1979.

Index categories: Shock Waves and Detonations; Research Facilities and Instrumentation.

*Senior Scientist, McDonnell Douglas Research Laboratories. Associate Fellow AIAA.

†Senior Engineer, McDonnell Aircraft Company. Member AIAA.